A procedure for evaluating the SOH of Li-ion batteries from data during the constant voltage charge phase and the use of an ECM with internal resistance

Angel Ivan Rodriguez-Cea[a], Daniel Morinigo-Sotelo[b], Francisco V. Tinaut[c,1]

[a] School of Industrial Engineering, Universidad de Valladolid, Paseo Prado de la Magdalena 3-5, E-47001 Valladolid, Spain

[b] Institute of Advanced Production Technologies (ITAP), Universidad de Valladolid, Paseo del Cauce, 59, E-47011 Valladolid, Spain

[c] Institute CMT-Clean Mobility and Thermofluids, Universitat Politècnica de València, Camino de Vera s/n, E-46022 Valencia, Spain

ABSTRACT

Lithium-ion batteries (LIBs) are present in virtually all sectors: communications, leisure, transportation, and even energy distribution. However, LIBs are affected by various ageing processes that cause a deterioration in their performance and can pose safety risks during operation. Therefore, it is vital to determine the State of Health (SOH) of the battery without affecting its regular operation. This paper presents a procedure for estimating and diagnosing the SOH of LIBs from data recorded during Constant Voltage (CV) phase charging. The developed method is based on specific battery parameters experimentally obtained and provides accurate results of the internal resistance and battery capacity. One of the advantages of the proposed procedure is that it can provide battery SOH results just from the value of only one measured point of current intensity during charging in the CV phase once some characteristic parameters of the battery are previously determined. Two NCA lithium batteries of different geometry (18650 and 26650) have been used in the diagnostics. The results of the proposed procedure have been validated experimentally, demonstrating high accuracy and fit. The proposed method can be implemented in a BMS to determine the SOH of the battery using the values of current intensity during a standard LIB charge.

Keywords: State of Health, Li-ion battery, Equivalent circuit model

Abbreviations and notations

BMS	Battery Management System	LIB	Lithium Ion Battery
CC	Constant Current	Q_{bat}	Battery capacity
CCCT	Constant Current Charge Time	$Q_{bat,n}$	Battery capacity at cycle n
CC-CV	Constant Current – Constant Voltage	$Q_{bat,n,50\%}$	Battery capacity at cycle n at 50% SOC
CV	Constant Voltage	R_{int}	Internal resistance
CVCT	Constant Voltage Charge Time	$R_{int,n}$	Internal resistance at cycle n
ECM	Equivalent Circuit Model	SOC	State of Charge

[1] Corresponding author.
E-mail address: ftinaut@mot.upv.es (Francisco V. Tinaut).

EIS	Electrochemical Impedance Spectroscopy	SOH	State of Health
EV	Electric Vehicle	V_{oc}	Open Circuit Voltage
HI	Health Indicator	V_t	Terminal Voltage

1. Introduction

Lithium-ion batteries (LIBs) are ubiquitous in virtually every field: communications, leisure, transportation, and power distribution. The deployment of electric vehicles (EVs) over the last decade has positioned LIBs as the preferred energy storage system in powertrain applications [1], [2], [3] due to their high energy capacity (up to 300 Wh/kg), high performance, no memory effect, and long lifetime [4]. Due to the high requirements of the batteries used in EVs, they are usually replaced when they reach 80% of the nominal capacity [5], [6]. However, the retired batteries can be used in other less demanding sectors, such as, for example, power applications in electrical networks with strong penetration of renewable generation [7].

The loss of performance of LIBs in EVs is mainly due to cycling ageing, a complex phenomenon involving chemical and physical mechanisms that can be grouped into three categories: Loss of Lithium Inventory (LLI), Loss of Active Material (LAM), and Increased Internal Resistance (IRI) [8], [9]. To quantify ageing, several Health Indicators (HI), such as battery storage capacity (Q_{bat}) or internal resistance (R_{int}), are used [10]. From these two indicators, the State of Health (SOH) can be defined in terms of the ratio between the current capacity and the nominal capacity (SOH_Q) or the ratio between the resistance of the battery and the nominal resistance (SOH_R) [11], [12], [13].

Monitoring SOH allows efficient battery use and avoids safety risks during battery operation, so testing routines in the *Battery Management System* (BMS) equipment should be included. SOH estimation methods are usually classified into three groups: direct measurement methods, model-based methods, and data analysis-based methods [14], [15], [16]. Direct measurement-based methods calculate capacitance by charge counting or Coulomb counting, while internal resistance is determined by pulsed discharge or Electrochemical Impedance Spectroscopy (EIS) [12], [17], [18]. These types of measurement require specialised equipment data acquisition systems incompatible with normal battery use. Model-based methods avoid the disadvantages of direct measurement techniques and accurately calculate the capacity, resistance and other characteristics associated with battery deterioration through equivalence circuit modelling (ECM) or adaptive filters [13]. Finally, data-driven methods consider the battery as a black box and use methods such as Fuzzy Logic (FL) or Neural Networks (NN) to estimate SOH. The drawback of these methods is the large database and training required to perform the results correctly [16], [19].

A practical method of SOH estimation should be compatible with typical EV battery use and should not require complex testing. The regular process of LIB discharging and complete charging provides sufficient information to estimate the SOH by analysing Incremental Capacity (IC) and Differential Voltage (DV) [20], [21], [22]. Other research proposes to estimate the SOH from different alternatives: the constant current charging process [23], the full charging process [24], and four characteristic geometrical parameters of the charge curves [25]. Also noteworthy are the proposals of [26] and [27], which are based on the use of a Constant Current Charge Time (CCCT) and a Constant Voltage Charge Time (CVCT) from the duration of the Constant Current

(CC) and Constant Voltage (CV) charging phase, respectively. However, the above methods require all the data from the charging process in the CC phase. In typical operation, EV batteries are rarely discharged and fully charged, and data may be affected by incomplete predischarge [28], [29]. For this reason, SOH estimation methods that only use data from the CV charging phase are more robust than those that involve the CC charging phase. This is demonstrated by [30], which verified that 5.5% of the lithium loss occurred in the CC charging mode and 94.5% in the CV charging mode. The phenomena studied by [29] shows that the shape of the CV phase charging current curve varies with respect to the SOH of the battery. Furthermore, [31] relates battery capacity loss to CV phase charging and proposes a correlation between model parameters, battery capacity, and SOH.

As ECMs can be easily implemented in *online* SOC estimation applications, they can also be applied to determine SOH from measurements during the CV phase. With this premise, several authors, such as [28], [29], [32], and [33], have formulated mathematical expressions for the CV charge current using an internal resistance ECM to obtain battery SOH, associating the physical meaning to the model parameters.

This paper introduces an approach for estimating the State of Health (SOH) using an internal resistance ECM. This method is well-suited for integration into a BMS in a lithium-ion battery. The procedure has been validated through experiments, in which the estimation of SOH was carried out by monitoring the increase in internal resistance and the decrease in storage capacity of two batteries during their ageing process, even when their residual capacity was very low.

The organisation of the manuscript is as follows: In Section 2, the ECM is used to characterise the CV charge curve and presents the procedure developed for simulation and performance. Section 3 details the equipment and procedure for characterising and performing the ageing tests. Section 4 presents the procedure's parameterisation and the results obtained with the proposed method for the same battery. In Section 5, the developed procedure is applied to two battery cells throughout their lifetime, and the obtained results are compared with the respective initial performances. Finally, section 6 shows the conclusions and the advantages of the proposed methodology.

2. Development of the proposed procedure

To accurately describe the dynamic characteristics of a battery, a theoretical equivalent circuit model (ECM) ideally includes a series resistor and an infinite number of resistor-capacitor (RC) groups [34]. However, in many cases, a model with one or two RC groups is sufficient to obtain satisfactory results with respect to the computational effort required for calculating nonstationary currents [35]. Even an ECM with a variable voltage source and a single internal resistor is enough to reproduce the behaviour of a battery during the CV charging phase, given the slow change of the current with time. Therefore, this model offers a practical balance between simplicity and quality of results.

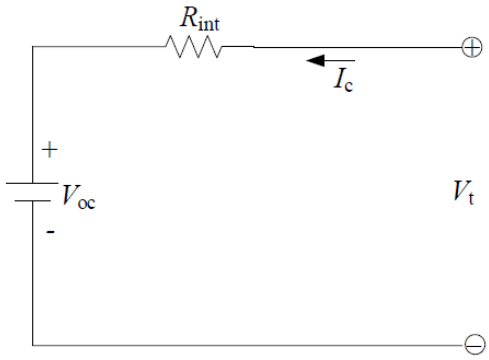

Figure 1. Schematic of the internal resistance ECM model used.

The schematic of the internal resistance ECM used is shown in Figure 1. It comprises a voltage source representing the open circuit voltage (V_{oc}) and an ohmic resistance in series (R_{int}). In this case, because the behaviour of the charge is studied in the constant voltage (CV) phase, V_{oc} and R_{int} are defined as time-dependent variables. Furthermore, considering the battery's life cycle stages, denoted by the index 'n' representing the number of control cycles studied within the ageing process, variables that change with the State of Health (SOH) are labeled with that index. Therefore, n = 0 corresponds to the new battery, with 'n' increasing after each ageing cycle. With these considerations, the ECM model behaviour is expressed as follows.

$$V_{oc}(t) + R_{int,n}(t) \cdot I_c(t) = V_t(t) \quad (1)$$

In Equation (1, V_t represents the terminal voltage of the battery, Voc represents the open circuit voltage, Rint,n is the internal resistance of the battery in the corresponding control cycle, and I_c is the current flowing through the battery, with positive values during the charging phase and negative values during the discharging phase.

The state of charge (SOC) of the battery under study can be calculated from the charge count indicated in Equation 2, where $Q_{bat,n}$ is the capacity of the battery during the charging or discharging process of the battery in cycle n. This capacity is considered constant within the cycle studied but variable between different charging and discharging cycles.

$$SOC\ (t) = \int_0^t \frac{I_c(t)}{Q_{bat,n}}\, dt \quad (2)$$

Furthermore, for each LIB, there is a characteristic relationship (indicated in Equation 3) between the open circuit voltage (V_{oc}) and the state of charge SOC that remains unaffected by battery ageing [32].

$$SOC\ (t) = SOC\left(V_{oc}(t)\right) \quad (3)$$

During the usual CC-CV charging process, the SOC increases within the CV charging phase, accompanied by an increase in V_{oc}. Consequently, to maintain the terminal voltage (V_t) at the maximum value, $V_{t,max}$ (as per the manufacturer's LIB specifications), the charging current (I_c) must be progressively reduced. Substituting the terms of Equation 1, it is possible to model the CV charging process, as shown in Equation 4.

$$V_{oc}(t) + R_{int,n}(t) \cdot I_c(t) = V_{t,max} \tag{4}$$

Equation 5 is derived by applying the adapted ECM model to the CV charging process, as indicated in Equation 4, and incorporating the functional dependencies between V_{oc} and SOC outlined in Equations 2 and 3. This Equation is presented in differential form to facilitate the simplification process leading to Equation 6.

$$\frac{dSOC}{dV_{oc}}\left(-R_{int,n}(t) \cdot \frac{dI_c(t)}{dt} - \frac{dR_{int,n}(t)}{dt} \cdot I_c(t)\right) = \frac{I_c(t)}{Q_{bat,n}} \tag{5}$$

$$\frac{dI_c(t)}{I_c(t)} = -\frac{\frac{dSOC}{dV_{oc}} \cdot \frac{dR_{int,n}(t)}{dt} + \frac{1}{Q_{bat,n}}}{\frac{dSOC}{dV_{oc}} \cdot R_{int,n}(t)} dt \tag{6}$$

Until now, no further simplifications have been necessary beyond accepting the ECM model as valid. However, to apply this procedure numerically in the CV charging phase of cycle n, it is beneficial to consider $Q_{bat,n}$ as a constant value. Moreover, the functions SOC(V_{oc}) and $R_{int,n}$(t) can be approximated as linear functions over time, given that their variations are minimal relative to time when SOC >70%.

During the CV charge phase, the SOC is large and increases with V_{oc} until it reaches the corresponding limiting values: SOC = 100% and $V_{oc} = V_{t,max}$. Under these conditions, SOC(Voc) can be assumed to exhibit linear behaviour with V_{oc}. This dependence can be experimentally verified during the initial battery characterisation. In fact, only the slope of this linear function is relevant in this procedure, denoted in Equation 6 as $\frac{dSOC}{dV_{oc}}$, which proves to be a constant, positive value.

Additionally, the internal resistance $R_{int,n}$ depends on the SOC, albeit with slight variations due to battery ageing in each cycle. To address this variation analytically, it is assumed that in the CV charging process $R_{int,n}$ increases linearly with time and can be expressed as shown in Equation 7. Here, the slope of the function, denoted as 'a', remains independent of battery ageing, while the constant term 'bn' changes with battery ageing. However, it is more convenient to study the evolution of the battery's internal resistance by normalising the term 'b_n' to the internal resistance value at 50 % SOC in a given control cycle n ($R_{int,n,50\%}$). In this case, the cycle-dependent term 'b_n' is replaced by a coefficient 'b', which remains invariant with ageing, as indicated in Equation 8.

$$R_{int,n}(t) = a \cdot t + b_n \tag{7}$$

$$R_{int,n}(t) = a \cdot t + b \cdot R_{int,n,50\%} \tag{8}$$

To integrate the differential Equation 6, the linearisation of the functions SOC(V_{oc}) and $R_{int,n}$(t) previously mentioned are taken into account, as well as the phase of the CC-CV charging process in which it occurs. Therefore, the initial condition (t=0) has been set as the transition from the constant current (CC) charging phase to the constant voltage (CV) charging phase. Therefore, the current at the instant t = 0 is the current maintained during the previous CC charging phase (I_{cc}).

Equation 9, valid during the charging process in the CV phase, shows the analytical relationship between I_c(t) and the relevant battery parameters. In Equation 9 there are variables independent of aging (a, b, $dSOC/dV_{oc}$) while others are dependent on battery ageing ($R_{int,n,50\%}$, $Q_{bat,n}$). In other words, Equation 9 allows for calculating the constant voltage phase charging current for a battery with a given ageing state (as given by $R_{int,n,50\%}$ and $Q_{bat,n}$).

$$I_c(t) = I_{cc} \cdot \left(1 + \frac{a \cdot t}{b \cdot R_{int,n,50\%}}\right)^{-\left(1+\frac{1}{\frac{dSOC}{dV_{oc}} \cdot a \cdot Q_{bat,n}}\right)} \tag{9}$$

When the charge current I_c(t) is recorded experimentally, these data can be used in the model developed to determine the battery condition by obtaining one of the two ageing dependent variables. If the battery capacity $Q_{bat,n}$ is known, the internal resistance $R_{int,n,50\%}$ can be calculated mathematically from Equation 9. This result in Equation 10, the mathematical expression of the diagnostic procedure for the internal resistance at 50 % SOC of the battery in the control cycle n.

$$R_{int,n,50\%} = \frac{I_c(t) \cdot a \cdot t}{b \cdot \left(I_{cc} \cdot \left(\frac{I_c(t)}{I_{cc}}\right)^{\frac{1}{\frac{dSOC}{dV_{oc}} \cdot a \cdot Q_{bat,n}+1}} - I_c(t)\right)} \tag{10}$$

Similarly, if the internal resistance $R_{int,n,50\%}$ is known, solving Equation 9 for the battery capacity $Q_{bat,n}$ provides the mathematical expression of the diagnostic procedure for the battery capacity at control cycle n, as indicated in Equation 11.

$$Q_{bat,n} = -\frac{\ln\frac{R_{int,n,50\%} \cdot b + a \cdot t}{R_{int,n,50\%} \cdot b}}{\frac{dSOC}{dV_{oc}} \cdot a \cdot \left(\ln\frac{I_c(t)}{I_{cc}} + \ln\frac{R_{int,n,50\%} \cdot b + a \cdot t}{R_{int,n,50\%} \cdot b}\right)} \tag{11}$$

3. Experimental methodology for battery ageing and measurement

3.1. Experimental setup: batteries and test bench

Two different types of lithium-ion batteries, both Panasonic brand and NCA type, have been used: one NCR18650B battery with a 3100 mAh capacity and another NCR26650A battery with a 5000 mAh capacity. Both batteries have been subjected to the same initial characterisation procedure and subsequent ageing test with the electric current values recommended by the manufacturer. The specifications of the batteries used in the tests are shown in **Error! Not a valid bookmark self-reference.**.

Table 1. Batteries specifications

Battery	**NCR18650B**	**NCR26650A**
Type	NCA	NCA
Rated capacity	3100 mAh	5000 mAh
Rated voltage	3.7 V	
Maximum voltage	4.2 V	
Minimum voltage	2.6 V	
Maximum discharge intensity	2 C	1 C
Maximum charge intensity	0.5 C	

A test bench, consisting of an iTech IT6723 programmable voltage source, an iTech IT8512A+ programmable electronic load, and a computer with LabView software for control and data storage, was utilised for the experimentation. Additionally, the test bench includes a system for acquiring voltage, current, and temperature measurements, which are also recorded on the computer. The test bench setup is shown in Figure 2.

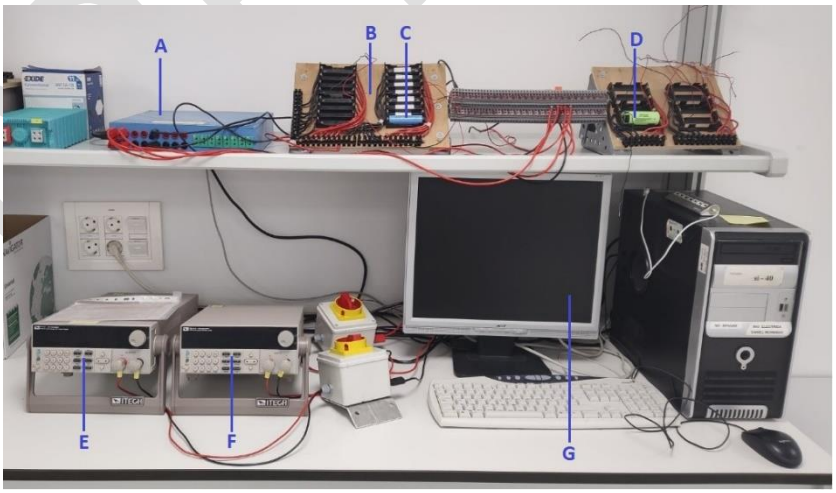

Figure 2. General view of the battery test bench. (A) Measurement acquisition system, (B) battery mount, (C) LIB NCR18650B, (D) LIB NCR26650A, (E) iTech IT6723 programmable power supply, (F) iTech IT8512A+ programmable electronic load, (G) computer with LabView software.

The batteries studied have been placed in battery holders designed for each battery's dimensions, following standards for 18650 and 26650 batteries. These battery holders include

direct voltage measurement sockets on the terminals to ensure that measurements are not affected by voltage drops in the test bench's power conductors during the charging and discharging processes.

All battery tests were performed at ambient temperature (laboratory climate control set at 22 ± 3ºC). Data acquisition systems, including voltage, current and temperature, were configured with a sampling frequency of 1 Hz. In the test bench control system, the shutdown conditions were set to the manufacturer's maximum and minimum voltage values for each battery.

3.2. Procedure for battery ageing and characterisation test

The test procedure, shown in Figure 3, has been designed to simulate the continuous use of the batteries at nominal values indicated by the manufacturer. The test procedure has three distinct parts: 1 - initial characterisation, 2 - condition monitoring, and 3 - controlled ageing.

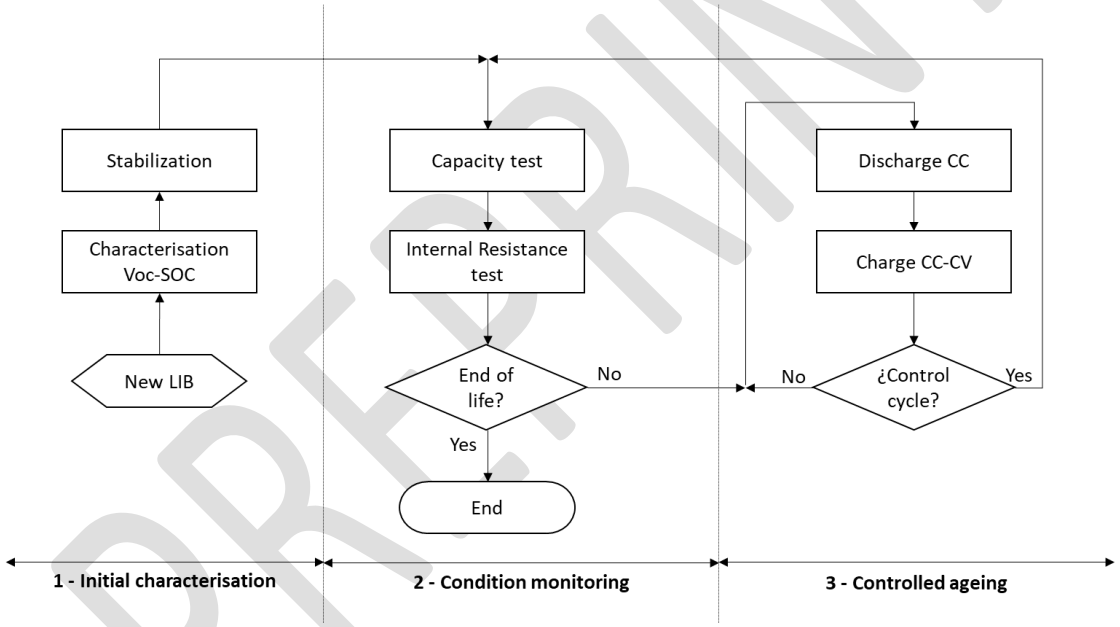

Figure 3. Experimental flow chart

The initial characterisation is the first test to be performed. The objective of this test is to extract the battery's characteristic parameters and compare them with those provided by the manufacturer. The battery is first fully charged and discharged to stabilise it and then slowly discharged and charged at a rate of 0.02 C to obtain the characteristic V_{oc}(SOC) function of the battery.

During the condition check, the battery's capacity and internal resistance are compared with historical data, if available. If the battery is new, this data is recorded for future comparisons. After controlled ageing, the recorded data is analysed to see how the parameters change with planned ageing.

Condition monitoring tests consist of a discharge and a charge under nominal conditions to verify battery capacity and, subsequently, a discharge and a pulse charge to determine the internal

resistance. The data collected in these tests are analysed to determine whether or not the battery under study has reached end-of-life conditions according to the criteria used in the automotive industry, as indicated in section 1.

A complete discharge is conducted to verify the battery capacity. The procedure begins with the battery fully charged at 100 % SOC, and it is discharged at a constant current of 1 C until the minimum voltage value is reached; at this point, SOC is considered 0 %. Subsequently, the battery is fully charged using the CC-CV procedure with an initial charge current of 0.5 C. Battery capacity is determined as the average value of the values recorded between discharge and charge.

To determine the battery's internal resistance, a discharge and charge are carried out with intensity pulses. The procedure begins with the battery fully charged at 100 % SOC, and it is discharged using constant intensity pulses (0.5 C - 600 seconds) until reaching the minimum voltage value established for each battery (2.6 V). Between pulses, the battery is allowed to stabilise for 900 seconds. Subsequently, the battery is fully charged using the CC-CV procedure by applying 0.5 C pulses.

If the test results and verifications indicate that the battery has reached the end of its useful life, controlled ageing is stopped. However, if the battery has not depleted its characteristics, the controlled ageing stage begins or restarts as needed.

In the controlled ageing stage, the battery is cycled according to the nominal conditions specified by the manufacturer. 100 charge and discharge cycles are performed automatically, and then a status check is performed. Battery charging is carried out according to the CC-CV protocol at an initial rate of 0.5 C and a cutoff of 0.02 C. The battery is discharged at a constant current with a rate of 1 C until the minimum voltage indicated by the battery manufacturer is reached. The computer system records the number of cycles performed during the process and monitors battery voltage, current, and temperature, stopping the cycling process if any of these indicators exceed the safety values.

Figure 4 demonstrates that the NCR18650B battery reached the 80 % threshold of its rated capacity after 500 charging cycles, whereas the NCR26650A battery achieved this threshold after 256 cycles. This comparison underscores the distinct durability and performance attributes between the two battery types from the same manufacturer and composition. Despite surpassing the 80% limit, it was decided to try to reach the same number of cycles for both batteries.

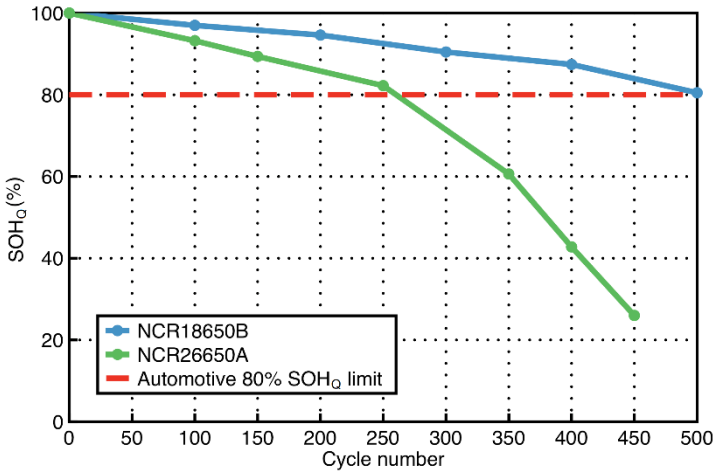

Figure 4. SOH$_Q$ evolution during the tests for NCR18650B (blue) and NCR26650A (green). In red is indicated the 80% SOH$_Q$ limit used in automotive industry.

4. Experimental validation of the developed procedure

The procedure developed in section 2 is applied to the experimental data of the NCR18650B battery. The necessary variables are extracted and manipulated in simulation mode, and the results are compared with the experimental data. This comparison is conducted at six control points, strategically chosen to cover the entire useful life of the battery: 0, 100, 200, 300, 400 and 500 cycles. These control points provide a comprehensive view of the battery's performance over time, allowing us to assess the accuracy of the results using several criteria.

4.1. Obtaining battery parameters from a standard charging process

The internal resistance is modelled using the manufacturer's technical sheet's initial value ($R_{int,0}$) and the experimentally determined value at 50 % of SOC ($R_{int,n,50\%}$) after an arbitrary number of ageing cycles. The internal resistance is assumed to behave linearly overtime during the CV charging phase. This trend has been observed in the tested batteries during the experimental charges, as shown in Figure 5. In the figure, the slope of the internal resistance remains constant while the independent term increases with the ageing cycles, causing the internal resistance curves during the CV charging phase to shift vertically but with a similar slope.

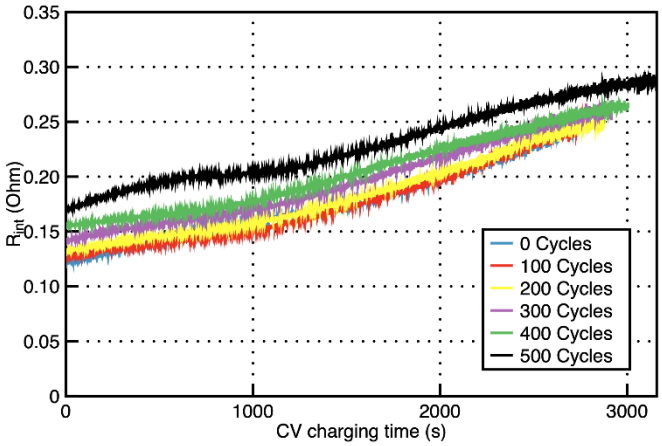

Figure 5. Evolution of the experimental internal resistance during CV phase charging in the different control cycles for NCR18650B.

Equation 12 is obtained by calculating the average value of the linearization coefficients of the internal resistance of the different control points, the ratio of the V_{oc} and the charge intensity during the CV phase, and normalizing to the value of 50 % SOC.

$$R_{int,n}(t) = 3.99 \cdot 10^{-5} \cdot t + 2.21 \cdot R_{int,n,50\%} \quad (12)$$

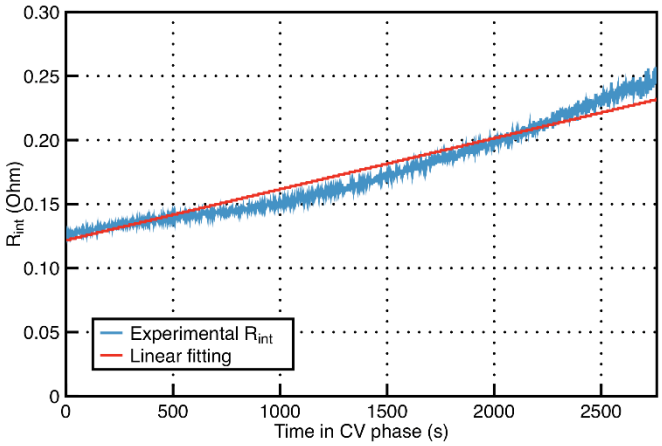

Figure 6. Comparison between internal resistance during the CV charging phase of the NCR18650B battery at the 100th cycle control point (red) and the linear function proposed in the equation 12 for the same control point (blue).

The characteristic function V_{oc}(SOC) is obtained during the battery's initial characterisation. Its inverse function SOC(V_{oc}) is calculated from these values. It is important to note that the characteristic function V_{oc}(SOC) and its inverse SOC(V_{oc}) remain invariant throughout the battery lifetime and are not affected by ageing processes, as indicated by [32]. Additionally, the CV charging phase corresponds to the last part of the SOC(V_{oc}) curve, where the SOC is high (usually, SOC > 70 %). In this interval, the V_{oc} increases rapidly and monotonically and can be assumed linear during the CV charging phase [29], as shown in Equation 13. Both statements can be verified in Figure 7, where the SOC(V_{oc}) functions are compared for 0 and after 450 cycles.

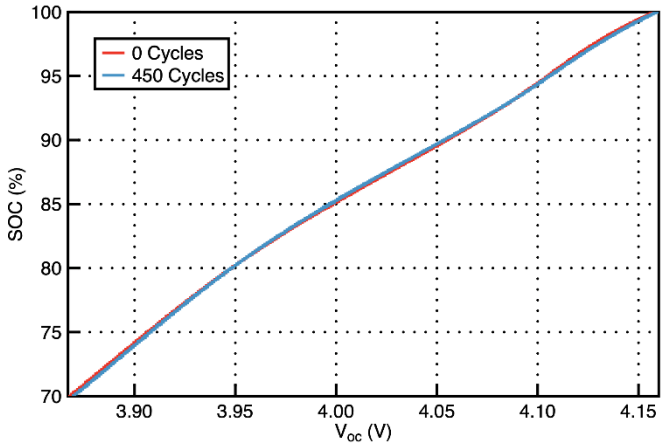

Figure 7. Characteristic relationship between SOC and V_{oc} for NCR18650B at 0 cycles (red) and after 450 cycles (blue).

$$SOC(V_{oc}) = 0.966 \cdot V_{oc} - 3.015 \quad (13)$$

Performing the derivative of Equation 13 the slope $dSOC/dV_{oc}$ is obtained, which is necessary for Equations 9, 10 and 11, the general form of the procedure for simulation and diagnostics procedures. As mentioned before, SOC(V_{oc}) exhibits a linear behaviour, with a slope that remains constant throughout its expected lifetime.

The rest of the input variables are immediately available. I_{cc}, $Q_{bat,0}$, and $R_{int,0,50\%}$ are specified by the manufacturer. The variables $Q_{bat,n}$ and $R_{int,n,50\%}$ for each control point are obtained according to the test procedure indicated in Section 3. Table 2 specifies the values of the input variables used for the NCR18650B cell.

Table 2: Input variables for NCR18650B

Input variable	0 cycles	100 cycles	200 cycles	300 cycles	400 cycles	500 cycles
I_{cc} (A)	3.20					
$dSOC/dV_{oc}$	0.966					
$R_{int,n,50\%}$ (Ω)	0.052	0.055	0.058	0.061	0.064	0.075
$Q_{bat,n}$ (Ah)	3.100	2.986	2.916	2.785	2.692	2.478

4.2. Comparison of theoretical and experimental results

With the input variables indicated in Table 2, the charging current curve in the CV phase for the battery state control points 0, 100, 200, 300, 400, and 500 cycles has been simulated using Equation 9. The results obtained in the simulation are shown and compared with the experimentally recorded charging current for each control point, as shown in Figure 8.

Two goodness criteria are used to analyse the similarity between the experimental electric current curve and the one calculated by the proposed procedure: Root Mean Square Error (RMSE) and the Correlation Coefficient R2. For RMSE, a value close to zero indicates a better fit of the results to the experimental data, while for R, it has to be close to unity.

As shown in Table 3, the indicators obtained reveal that for the six NCR18650 battery control points studied, the RMSE value is on the order of hundredths, indicating proximity to zero, and R^2 is close to unity. Therefore, based on the error indicators in Table 3 and the results displayed in Figure 8, it can be concluded that the estimated electric current using the proposed procedure aligns well with the experimentally obtained values for the constant voltage charging process.

Table 3. Similarity indicators between the experimental intensity and the simulation results for NCR18650B.

Cycle #	**0**	**100**	**200**	**300**	**400**	**500**
RMSE (A)	0.0231	0.0289	0.0221	0.0220	0.0164	0.0188
R^2 (-)	0.9989	0.9984	0.9992	0.9996	0.9998	0.9998

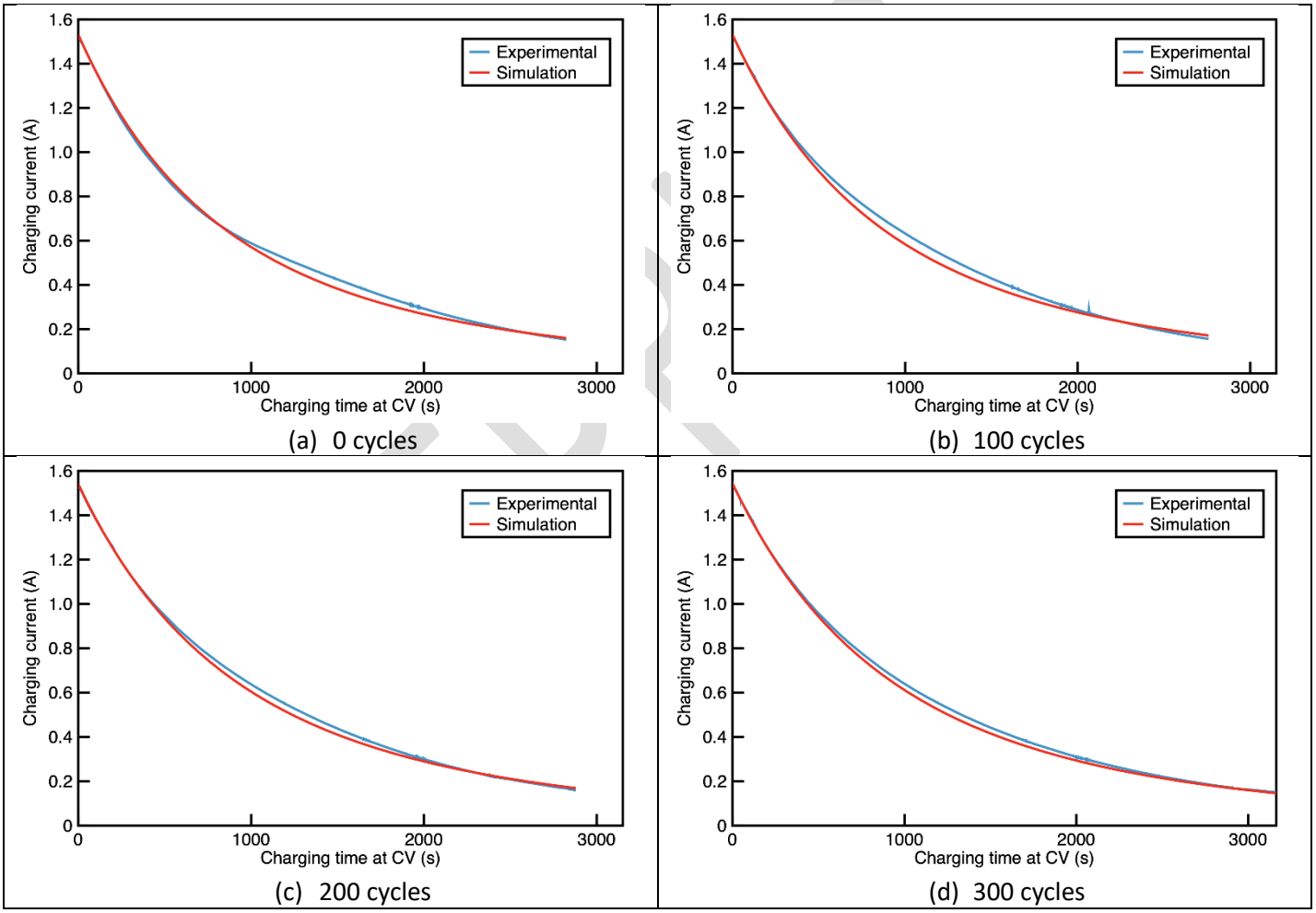

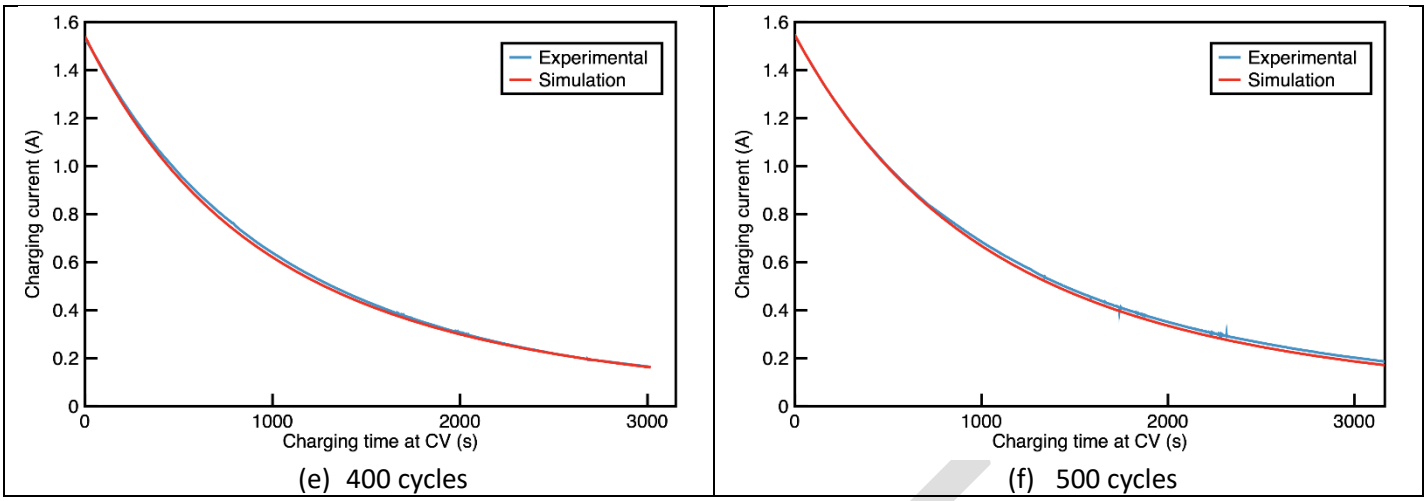

Figure 8. Comparison between experimental charging intensity (blue) and simulation result (red) for NCR18650B at different control points.

5. Application of the procedure to determine battery SOH

The internal resistance ($R_{int,n,50\%}$) or the battery capacity ($Q_{bat,n}$) can be used to keep track of battery ageing. From these two values, two alternative expressions of battery SOH can be defined, as indicated in Section 1, and shown in Equations 14 (SOH_R) and 15 (SOH_Q) respectively:

$$SOH_R = \left(1 - \frac{R_{int,n,50\%} - R_{int,0,50\%}}{R_{int,0,50\%}}\right) \cdot 100 \quad (14)$$

$$SOH_Q = \frac{Q_{bat,n}}{Q_{bat,0}} \cdot 100 \quad (15)$$

To calculate SOH_R, it is necessary to know the evolution of the battery's internal resistance after the ageing process. For this purpose, equation 10 is used, which provides the internal resistance at 50 % SOC ($R_{int,n,50\%}$). From it, SOH_R is obtained by Equation 14.

Similarly, to obtain the value of the aged battery capacity, Equation 11 is used, which provides the battery capacity at the control point where the diagnosis is performed. Using this result in Equation 15, SOH_Q is obtained.

The proposed diagnostic procedure offers a significant advantage in not requiring the complete set of experimental data on charge current during the CV phase. Diagnosis of the LIB can be conducted by using only some specific points from the CV charging process (in the limit, one point). When the entire set of registered charge current values is available, numerous (although similar for a given ageing cycle) internal resistance and capacity values can be obtained. These results can be further processed to enhance the accuracy of the procedure.

The results obtained for internal resistance $R_{int,n,50\%}$ and capacity $Q_{bat,n}$ for the NCR18650B and NCR26650A batteries are indicated in Table 4 and Table 5, respectively. $R_{int,n,50\%}$ and $Q_{bat,n}$ have been calculated for the complete data set recorded during the CV charging phase, obtaining as

many results as recorded data. Subsequently, the average value obtained for all the results is compared with the value obtained experimentally during the LIB diagnostic phase at each control point according to the procedure indicated in Section 3 and the similarity between both is evaluated using RMSE.

It can be observed in Table 4 and Table 5 how $R_{int,n,50\%}$ increases while $Q_{bat,n}$ decreases as the ageing cycling of the two batteries studied increases. The low value of RMSE obtained for $R_{int,n,50\%}$ confirms that the developed procedure provides consistent values that allow it to diagnose LIB quickly and easily. The order of magnitude difference in RMSE obtained between $R_{int,n,50\%}$ and $Q_{bat,n}$ is a consequence of the dependent terms of the natural logarithm existing in Equation 11.

Table 4. Summary and comparison of diagnostic results for the NCR18650B battery.

NCR18650B	$R_{int,n}(50\ \%)$ **(Ω)**			$Q_{bat,n}$ **(Ah)**		
Control cycle	**Experimental**	**Diagnosis**	**RMSE**	**Experimental**	**Diagnosis**	**RMSE**
100	0.055	0.057	0.0043	2.986	3.057	0.2697
200	0.058	0.059	0.0030	2.916	3.007	0.1860
300	0.061	0.062	0.0028	2.785	2.903	0.1545
400	0.064	0.065	0.0029	2.692	2.769	0.1481
500	0.075	0.077	0.0027	2.478	2.564	0.1225

Table 5. Summary and comparison of diagnostic results for the NCR26650A battery.

NCR26650A	$R_{int,n}(50\ \%)$ **(Ω)**			$Q_{bat,n}$ **(Ah)**		
Control cycle	**Experimental**	**Diagnosis**	**RMSE**	**Experimental**	**Diagnosis**	**RMSE**
250	0.056	0.059	0.0058	4.411	4.593	0.2231
350	0.068	0.070	0.0027	3.259	3.375	0.1406
400	0.090	0.092	0.0048	2.307	2.351	0.1438
450	0.098	0.108	0.0165	1.842	1.637	0.2687

Table 6 and Table 7 show the SOH referred to the internal resistance (SOH_R) and the capacity (SOH_Q) calculated with the experimental data collected in the test bench and with the results obtained with the diagnostic procedure for the NCR18650A and NCR26650B batteries in each control cycle studied.

For both batteries, it can be observed that the SOH referred to the internal resistance (SOH_R) calculated from the results of the diagnostic procedure differs between 2 % and 5 % with respect to the calculation based on experimental data. For SOH_Q of both batteries, the same difference is observed between the results obtained experimentally and the diagnostic procedure. Despite the difference, the quality of the results obtained from the diagnostic procedure is adequate for use in BMS equipment.

The strongest discrepancy between the SOH_R values calculated with experimental data and with the diagnostic procedure appears at the 450th control cycle of NCR26650A (Table 7). The reason for this anomalous case is due to the excessive ageing degradation that the battery presented at that ageing cycle. This excessive degradation was already noticed at control cycle 250, but the tests were maintained to observe the evolution of SOH beyond that point (see Figure 4).

Table 6. Comparison of SOHR and SOHQ calculated with experimental and diagnostic data for NCR18650B

NCR18650B	SOH_R (%)		SOH_Q (%)	
Control cycle	Experimental	Diagnosis	Experimental	Diagnosis
100	94.2	90.4	96.3	98.6
200	88.5	86.5	94.1	97.0
300	82.7	80.8	89.8	93.6
400	76.9	75.0	86.8	89.3
500	55.8	51.9	79.9	82.7

Table 7 Comparison of SOHR and SOHQ calculated with experimental and diagnostic data for NCR26650A

NCR26650A	SOH_R (%)		SOH_Q (%)	
Control cycle	Experimental	Diagnosis	Experimental	Diagnosis
250	98.2	93.7	88.2	91.9
350	76.4	72.7	65.2	67.5
400	36.4	32.7	46.1	47.0
450	21.8	3.6	36.8	32.7

Table 6 and Table 7 show the SOH referred to the internal resistance (SOH_R) and the capacity (SOH_Q) calculated with the experimental data collected in the test bench and with the results obtained with the diagnostic procedure for the NCR18650A and NCR26650B batteries in each control cycle studied.

For both batteries, the SOH, referred to as the internal resistance (SOHR) calculated from the diagnostic procedure results, differs between 2 % and 5 % from the calculation based on experimental data. For the SOH_Q of both batteries, the same difference is observed between the results obtained experimentally and the diagnostic procedure. Despite the difference, the quality of the results obtained from the diagnostic procedure is adequate for use in BMS equipment.

The major difference between the SOH_R values calculated using experimental data and the diagnostic procedure is observed at the 450th control cycle of NCR26650A (Table 7). This anomalous case is due to the excessive ageing degradation that the battery presented during that ageing cycle. This excessive degradation was already noticed at control cycle 250, but the tests were maintained to observe the evolution of SOH beyond that point (see Figure 4).

6. Conclusions

In this paper, an SOH diagnostic procedure for LIB is proposed based on an internal resistance ECM model and using data recorded during a standard constant-voltage charging phase. The developed method uses specific parameters of the battery under inspection that can be easily obtained from the standard charge.

The RMSE indicators obtained both in the experimental validation, and those obtained in the applications demonstrate that the proposed procedure is accurate and adjusts to the experimental values.

The main novelty of the proposed procedure is its usefulness as a form of diagnosis to obtain the internal resistance and capacity of a LIB from the data recorded during charging in the CV phase.

Unlike other diagnostic procedures, having the full set of values of experimental current intensity $I_c(t)$ of the CV charging process is unnecessary. The procedure presented here can provide battery SOH results just from the value of a single point of the current during the charging CV phase once the characteristic parameters of the battery (a, b and $dSOC/dV_{oc}$) are previously determined. This greatly simplifies the diagnostic process and can be implemented on any BMS equipment.

Furthermore, using the value of the internal resistance at 50 % SOC ($R_{int,n,50\%}$) as a comparative parameter of internal resistance allows to simplify the diagnosis by unifying all the possible values of internal resistance that can be obtained in the range 0-100 % of SOC. This provides a reference value that changes with battery ageing and can be compared with the initial one provided by the manufacturer.

Although the battery's capacity can be known by performing a full charge, the proposed procedure also allows calculating the aged capacity value from the charging data in the CV phase and the internal resistance $R_{int,n,50\%}$.

Finally, the general form of the procedure allows simulation of the evolution over time of the charging electric current in the constant voltage phase for a given SOH, defined by the internal resistance and capacity of the battery. This can be useful in other areas such as training or component design.

CRediT authorship contribution statement

Angel Ivan Rodriguez-Cea: Writing – original draft, Methodology, Software, Investigation, Visualization, Methodology, Investigation, Data Curation, Formal analysis, Data curation. **Daniel Morinigo-Sotelo**: Writing – review & editing, Methodology, Validation, Formal analisis, Visualization, Supervision. **Francisco V. Tinaut**: Writing – review & editing, Conceptualization, Formal analisis, Resources, Supervision, Validation.

Declaration of competing interest

The authors declare that they have no known competing financial interests or personal relationships that could have appeared to influence the work reported in this paper.

Data availability

Data will be made available on request.

REFERENCES

[1] I. E. Agency, *Global EV Outlook 2020*. 2020. doi: https://doi.org/https://doi.org/10.1787/d394399e-en.

[2] S. B. Sarmah *et al.*, "A Review of State of Health Estimation of Energy Storage Systems: Challenges and Possible Solutions for Futuristic Applications of Li-Ion Battery Packs in Electric Vehicles," *J. Electrochem. Energy Convers. Storage*, vol. 16, no. 4, Nov. 2019, doi: 10.1115/1.4042987.

[3] X. Hu, C. Zou, C. Zhang, and Y. Li, "Technological Developments in Batteries: A Survey of Principal Roles, Types, and Management Needs," *IEEE Power Energy Mag.*, vol. 21, no. 2, pp. 52–63, Mar. 2023, doi: 10.1109/MPAE.2023.10083081.

[4] H. Li, “Practical Evaluation of Li-Ion Batteries,” *Joule*, vol. 3, no. 4, pp. 911–914, Apr. 2019, doi: 10.1016/j.joule.2019.03.028.

[5] P. Eleftheriadis *et al.*, “Second Life Batteries: Current Regulatory Framework, Evaluation Methods, and Economic Assessment,” in *2022 IEEE International Conference on Environment and Electrical Engineering and 2022 IEEE Industrial and Commercial Power Systems Europe (EEEIC / I&CPS Europe)*, IEEE, Jun. 2022, pp. 1–6. doi: 10.1109/EEEIC/ICPSEurope54979.2022.9854718.

[6] E. Hossain, D. Murtaugh, J. Mody, H. M. R. Faruque, M. S. Haque Sunny, and N. Mohammad, “A Comprehensive Review on Second-Life Batteries: Current State, Manufacturing Considerations, Applications, Impacts, Barriers & Potential Solutions, Business Strategies, and Policies,” *IEEE Access*, vol. 7, pp. 73215–73252, 2019, doi: 10.1109/ACCESS.2019.2917859.

[7] E. Michelini *et al.*, “Potential and Most Promising Second-Life Applications for Automotive Lithium-Ion Batteries Considering Technical, Economic and Legal Aspects,” *Energies*, vol. 16, no. 6, p. 2830, Mar. 2023, doi: 10.3390/en16062830.

[8] S. Ding, Y. Li, H. Dai, L. Wang, and X. He, “Accurate Model Parameter Identification to Boost Precise Aging Prediction of Lithium-Ion Batteries: A Review,” *Adv. Energy Mater.*, vol. 13, no. 39, Oct. 2023, doi: 10.1002/aenm.202301452.

[9] C. R. Birkl, M. R. Roberts, E. McTurk, P. G. Bruce, and D. A. Howey, “Degradation diagnostics for lithium ion cells,” *J. Power Sources*, vol. 341, pp. 373–386, Feb. 2017, doi: 10.1016/j.jpowsour.2016.12.011.

[10] W. Zhou, Q. Lu, and Y. Zheng, “Review on the Selection of Health Indicator for Lithium Ion Batteries,” *Machines*, vol. 10, no. 7, p. 512, Jun. 2022, doi: 10.3390/machines10070512.

[11] C.-P. Lin, J. Cabrera, F. Yang, M.-H. Ling, K.-L. Tsui, and S.-J. Bae, “Battery state of health modeling and remaining useful life prediction through time series model,” *Appl. Energy*, vol. 275, p. 115338, Oct. 2020, doi: 10.1016/j.apenergy.2020.115338.

[12] Z. Wang, X. Zhao, L. Fu, D. Zhen, F. Gu, and A. D. Ball, “A review on rapid state of health estimation of lithium-ion batteries in electric vehicles,” *Sustain. Energy Technol. Assessments*, vol. 60, p. 103457, Dec. 2023, doi: 10.1016/j.seta.2023.103457.

[13] S. K. Pradhan and B. Chakraborty, “Battery management strategies: An essential review for battery state of health monitoring techniques,” *J. Energy Storage*, vol. 51, p. 104427, Jul. 2022, doi: 10.1016/j.est.2022.104427.

[14] R. Xiong, L. Li, and J. Tian, “Towards a smarter battery management system: A critical review on battery state of health monitoring methods,” *J. Power Sources*, vol. 405, pp. 18–29, Nov. 2018, doi: 10.1016/j.jpowsour.2018.10.019.

[15] L. Chen, Z. Lü, W. Lin, J. Li, and H. Pan, “A new state-of-health estimation method for lithium-ion batteries through the intrinsic relationship between ohmic internal resistance and capacity,” *Measurement*, vol. 116, pp. 586–595, Feb. 2018, doi: 10.1016/j.measurement.2017.11.016.

[16] M. S. H. Lipu *et al.*, “A review of state of health and remaining useful life estimation methods for lithium-ion battery in electric vehicles: Challenges and recommendations,” *J. Clean. Prod.*, vol. 205, pp. 115–133, Dec. 2018, doi: 10.1016/j.jclepro.2018.09.065.

[17] N. Meddings *et al.*, “Application of electrochemical impedance spectroscopy to

commercial Li-ion cells: A review," *J. Power Sources*, vol. 480, p. 228742, Dec. 2020, doi: 10.1016/j.jpowsour.2020.228742.

[18] M. Berecibar, I. Gandiaga, I. Villarreal, N. Omar, J. Van Mierlo, and P. Van den Bossche, "Critical review of state of health estimation methods of Li-ion batteries for real applications," *Renew. Sustain. Energy Rev.*, vol. 56, pp. 572–587, Apr. 2016, doi: 10.1016/j.rser.2015.11.042.

[19] J. Wu, Y. Wang, X. Zhang, and Z. Chen, "A novel state of health estimation method of Li-ion battery using group method of data handling," *J. Power Sources*, vol. 327, pp. 457–464, Sep. 2016, doi: 10.1016/j.jpowsour.2016.07.065.

[20] J. Yang, Y. Cai, and C. Mi, "State-of-health Estimation for Lithium Iron Phosphate Batteries Based on Constant-voltage Charge Data Using a Resistor-inductor Network Based Equivalent Circuit Model," in *2021 IEEE Energy Conversion Congress and Exposition (ECCE)*, IEEE, Oct. 2021, pp. 1705–1711. doi: 10.1109/ECCE47101.2021.9595368.

[21] X. Li, J. Jiang, L. Y. Wang, D. Chen, Y. Zhang, and C. Zhang, "A capacity model based on charging process for state of health estimation of lithium ion batteries," *Appl. Energy*, vol. 177, pp. 537–543, Sep. 2016, doi: 10.1016/j.apenergy.2016.05.109.

[22] A. I. Pózna, K. M. Hangos, and A. Magyar, "Design of Experiments for Battery Aging Estimation," *IFAC-PapersOnLine*, vol. 51, no. 28, pp. 386–391, 2018, doi: 10.1016/j.ifacol.2018.11.733.

[23] D. Yang, X. Zhang, R. Pan, Y. Wang, and Z. Chen, "A novel Gaussian process regression model for state-of-health estimation of lithium-ion battery using charging curve," *J. Power Sources*, vol. 384, pp. 387–395, Apr. 2018, doi: 10.1016/j.jpowsour.2018.03.015.

[24] B. Xiao, B. Xiao, and L. Liu, "State of Health Estimation for Lithium-Ion Batteries Based on the Constant Current–Constant Voltage Charging Curve," *Electronics*, vol. 9, no. 8, p. 1279, Aug. 2020, doi: 10.3390/electronics9081279.

[25] C. Lu, L. Tao, and H. Fan, "Li-ion battery capacity estimation: A geometrical approach," *J. Power Sources*, vol. 261, pp. 141–147, Sep. 2014, doi: 10.1016/j.jpowsour.2014.03.058.

[26] Y. Zhang and B. Guo, "Online Capacity Estimation of Lithium-Ion Batteries Based on Novel Feature Extraction and Adaptive Multi-Kernel Relevance Vector Machine," *Energies*, vol. 8, no. 11, pp. 12439–12457, Nov. 2015, doi: 10.3390/en81112320.

[27] H. Liu *et al.*, "An analytical model for the CC-CV charge of Li-ion batteries with application to degradation analysis," *J. Energy Storage*, vol. 29, p. 101342, Jun. 2020, doi: 10.1016/j.est.2020.101342.

[28] W. Guo, L. Yang, Z. Deng, J. Li, and X. Bian, "Rapid online health estimation for lithium-ion batteries based on partial constant-voltage charging segment," *Energy*, vol. 281, p. 128320, Oct. 2023, doi: 10.1016/J.ENERGY.2023.128320.

[29] Z. Wang, S. Zeng, J. Guo, and T. Qin, "State of health estimation of lithium-ion batteries based on the constant voltage charging curve," *Energy*, vol. 167, pp. 661–669, Jan. 2019, doi: 10.1016/j.energy.2018.11.008.

[30] G. Ning, R. E. White, and B. N. Popov, "A generalized cycle life model of rechargeable Li-ion batteries," *Electrochim. Acta*, vol. 51, no. 10, pp. 2012–2022, Feb. 2006, doi: 10.1016/j.electacta.2005.06.033.

[31] A. Eddahech, O. Briat, and J.-M. Vinassa, “Determination of lithium-ion battery state-of-health based on constant-voltage charge phase,” *J. Power Sources*, vol. 258, pp. 218–227, Jul. 2014, doi: 10.1016/j.jpowsour.2014.02.020.

[32] J. Yang, B. Xia, W. Huang, Y. Fu, and C. Mi, “Online state-of-health estimation for lithium-ion batteries using constant-voltage charging current analysis,” *Appl. Energy*, vol. 212, pp. 1589–1600, Feb. 2018, doi: 10.1016/j.apenergy.2018.01.010.

[33] S. Zhang, S. Wu, G. Cao, and X. Zhang, “Capacity estimation for lithium-ion battery via a novel health indicator extracted from partial constant voltage charging curve,” *J. Clean. Prod.*, vol. 409, p. 137220, Jul. 2023, doi: 10.1016/j.jclepro.2023.137220.

[34] J. Lee, O. Nam, and B. H. Cho, “Li-ion battery SOC estimation method based on the reduced order extended Kalman filtering &,” vol. 174, pp. 9–15, 2007, doi: 10.1016/j.jpowsour.2007.03.072.

[35] X. Hu, S. Li, and H. Peng, “A comparative study of equivalent circuit models for Li-ion batteries,” *J. Power Sources*, vol. 198, pp. 359–367, 2012, doi: 10.1016/j.jpowsour.2011.10.013.